Saturation of curvature-induced secondary currents in relatively sharp bends: a two-dimensional modelling approach

T. Lazzarin & D.P. Viero
Dep. of Civil, Environmental and Architectural Engineering, Università di Padova, Padova, Italy

ABSTRACT: Secondary currents occurring in channel bends have manifold implications in river hydraulics. In reduced-order models, the typical parametrizations of helical flow assume their magnitude to increase linearly with the channel curvature, although this is valid only in mild-curvature bends. In sharper bends, the non-linear interaction between the primary and the secondary flow flattens the vertical profile of longitudinal velocity component, thus reducing the source mechanism of the secondary current. Established models for this so-called "saturation effect" all refer to the channel centreline. In this work, a pure 2D implementation of a saturation model is included in a Finite Element depth-averaged hydrodynamic model based on a Cartesian reference frame.

1 INTRODUCTION

In river bends, curvature-induced secondary currents are peculiar features of the flow field, with relevant consequences on a number of hydro- and morphodynamic processes (redistribution of momentum and shear stresses, bend scour, bar push and bank pull, mixing of suspended sediments and passive-tracers, etc.).

Parametrizations of the curvature-induced secondary flow have long been introduced in depth-averaged hydrodynamic models (either 1D or 2D). Under the hypothesis of mild-curvature bend, the magnitude of secondary flow is generally assumed to increase linearly with the streamline curvature, neglecting the mutual (non-linear) interaction among the primary and the secondary flow (Blanckaert & de Vriend, 2003; Yeh & Kennedy, 1993). However, experiments showed that, in the case of sharper bends, the growth of secondary flows beyond a certain point is hindered by a saturation mechanism (Blanckaert, 2009). Saturation emerges as a by-product of the momentum transfer promoted by the secondary flow itself: the helical flow induces a flattening on the vertical profile of longitudinal velocity, thus reducing the imbalance between centrifugal acceleration and hydrostatic pressure (i.e., the source of the secondary motion). The saturation of secondary current has been first assessed and modelled in an essentially 1D framework, which considers the mutual interaction among the longitudinal and the transversal components of velocity with reference to the channel axis (Blanckaert & de Vriend, 2010). In subsequent formulations, the saturation model has been extended to describe spanwise variations of the flow field using curvilinear, boundary-fitted computational grids, yet maintaining the centreline-based approach (Ottevanger, 2013; Qin et al., 2019), which implies limiting the model applicability to idealized meandering rivers.

Including effective parameterization of secondary currents in general-purpose 2D shallow water models is not straightforward. In real rivers, the channel geometry can change in time passing from bankfull to flood discharge, as well as in case of anabranching or braided rivers due to movable-bed dynamics, and the streamline curvature typically shows an unevenly spatial distribution. In such cases, the channel centreline, width, and the distance from bank, can change during a

single simulation, and are practically unknown from a pure 2D standpoint. The treatment of impervious banks for 2D computation of secondary flows is still an open issue (Blanckaert, 2001, Song et al., 2012).

In the present work, a pure 2D approach for secondary flows, which also accounts for non-linear saturation in relatively sharp bends, is proposed and implemented in a Finite Element, unstructured shallow water model based on a Cartesian (i.e., not curvilinear) reference frame. Dispersive terms in the depth-averaged Navier-Stokes equations account for the non-uniform vertical distribution of velocity, assuming a power-law and a linear vertical profile for longitudinal and transversal velocity, respectively. The intensity of secondary current is estimated by solving a transport equation to consider the helical flow inertia. A spatially-distributed dampening factor (expressed according to Blanckaert & de Vriend, 2003) reduces the vorticity production term when (and where) the secondary current is sufficiently developed, thus accounting for the non-linear saturation effect. Additional stresses at impervious banks are accounted for using a wall function. The model is validated against experimental data, and the importance of including the non-linear saturation model is demonstrated by comparison with results provided by the linear version of the model.

2 METHODS

2.1 *Model equations*

In a horizontal Cartesian frame with axes (x, y), the depth-averaged Navier-Stokes equations, also known as shallow water equations (SWEs), are (Defina, 2000):

$$\frac{D}{Dt}\left(\frac{q_x}{Y}\right) - \frac{1}{Y}\left(\frac{\partial Re_{xx}}{\partial x} + \frac{\partial Re_{xy}}{\partial y}\right) + \frac{1}{Y}\left(\frac{\partial D_{xx}}{\partial x} + \frac{\partial D_{xy}}{\partial y}\right) + \frac{\tau_{bx}}{\rho Y} + g\frac{\partial h}{\partial x} = 0 \tag{1}$$

$$\frac{D}{Dt}\left(\frac{q_y}{Y}\right) - \frac{1}{Y}\left(\frac{\partial Re_{xy}}{\partial x} + \frac{\partial Re_{yy}}{\partial y}\right) + \frac{1}{Y}\left(\frac{\partial D_{yx}}{\partial x} + \frac{\partial D_{yy}}{\partial y}\right) + \frac{\tau_{by}}{\rho Y} + g\frac{\partial h}{\partial y} = 0 \tag{2}$$

where t is time, D/Dt is the material (Lagrangian) total derivative, (q_x, q_y) are the depth-integrated velocity components, Y is the equivalent water depth (i.e., water volume per unit area), Re are the Reynolds stresses, (τ_{bx}, τ_{by}) are the bed stress components, h is the water surface elevation over a datum, ρ is the water density, and g is gravity. The dispersive stresses, D_{xx}, D_{xy} and D_{yy}, included in the SWEs to model the effects of non-uniform vertical distribution of velocity, are defined as:

$$\begin{aligned} D_{xx} &= \int_0^Y [u'(z)]^2\, dz \\ D_{xy} = D_{yx} &= \int_0^Y u'(z)v'(z)dz \\ D_{yy} &= \int_0^Y [v'(z)]^2\, dz \end{aligned} \tag{3}$$

where z is the vertical direction, and the apostrophe denotes the difference between the actual and the depth-averaged velocity components.

To obtain a close form of Eqs. (3), we consider a local (s, n) frame, with s and n denoting the streamwise and spanwise directions, respectively. The vertical profile of velocity is assumed power-law in the longitudinal direction, and linear with zero-mean in the transversal direction, as shown in Figure 1a (Begnudelli et al., 2010; Odgaard, 1986). Integration of Eqs. (3) leads to:

$$\begin{aligned} D_{ss} &= Y\frac{w^2}{m(2+m)} \\ D_{sn} = D_{ns} &= Y\frac{w\, v_{ns}}{1+2m}\mathrm{sign}(R) \\ D_{nn} &= Y\frac{(v_{ns})^2}{3} \end{aligned} \tag{4}$$

where w is the module of the depth-averaged velocity, m a friction parameter, v_{ns} the transversal velocity component at the free surface, and R the local radius of curvature of velocity streamlines (R is positive for clockwise bends in the flow direction, and negative vice-versa). The D_{xx}, D_{xy}, and D_{yy} terms are then obtained by rotation from the local (s, n) to the model (x, y) frame.

Dispersive stresses depend on the intensity of secondary flow, i.e. the streamwise vorticity component, which is here expressed in terms of transversal velocity component at the free-surface, v_{ns}. To account for the secondary flow inertia, a vorticity-transport approach is used, accounting for generation, transport, and dissipation of the streamwise component of vorticity, representing the helical flow intensity (Johannesson & Parker, 1989). Thus, v_{ns} is estimated by solving a depth-averaged vorticity equation in the form:

$$\frac{\partial v_{ns}}{\partial t} + \frac{\partial}{\partial x}\left(\frac{q_x v_{ns}}{Y}\right) + \frac{\partial}{\partial y}\left(\frac{q_y v_{ns}}{Y}\right) = f_D k_P \frac{w^2}{R} - k_D \frac{v_{ns} w}{Y} \tag{5}$$

with the production, k_P, and dissipation, k_D, coefficients defined according to the conservation principle used to estimate the magnitude of the helical flow (e.g., angular or spanwise linear momentum), and $f_D \in [0,1]$ the dampening factor which accounts for the non-linear saturation effect by reducing the production term. When $f_D = 1$, the mutual influence between the main and the secondary flow is neglected, thus obtaining a linear model (Camporeale et al., 2007; Song et al., 2012). According to Blanckaert & de Vriend (2003), f_D is a function of the bend parameter β as:

$$f_D = 1 - \exp\left(-\frac{0.4}{1.05\beta^3 - 0.89\beta^2 + 0.5\beta}\right) \tag{6}$$

$$\beta = \sqrt{\frac{Y}{|R|}}\left(\frac{0.41}{m}\right)^{-0.55}(\alpha+1)^{0.25} \tag{7}$$

$$\alpha = \frac{R}{w}\frac{\partial w}{\partial n} \tag{8}$$

being α the normalized transversal gradient of the depth averaged (longitudinal) velocity w.

As shown in Figure 1b, f_D decreases for larger values of Y/R since non-linear effects are amplified in sharper bends. f_D also depends on the velocity transversal gradient, α. Approaching a bend, the highest velocity thread locates at the inner side, i.e., $\alpha < 0$ and the helical flow production is the highest. As secondary currents develop along the bend, cross-stream momentum transfer shifts the high velocity thread to the outer side (thus increasing α) and flattens the vertical profile of the longitudinal velocity component, thus limiting the further increase of the helical flow intensity. Indeed, for increasing α, f_D decreases and limits the helical flow production term. In other words, α marks the transition from a potential ($\alpha = -1$) to a forced-vortex ($\alpha = 1$) flow pattern (Blanckaert & de Vriend, 2003), and changes the model behaviour from linear to non-linear accordingly.

In the model, α, β, and f_D vary in (x, y) and are computed on the based of the local flow features.

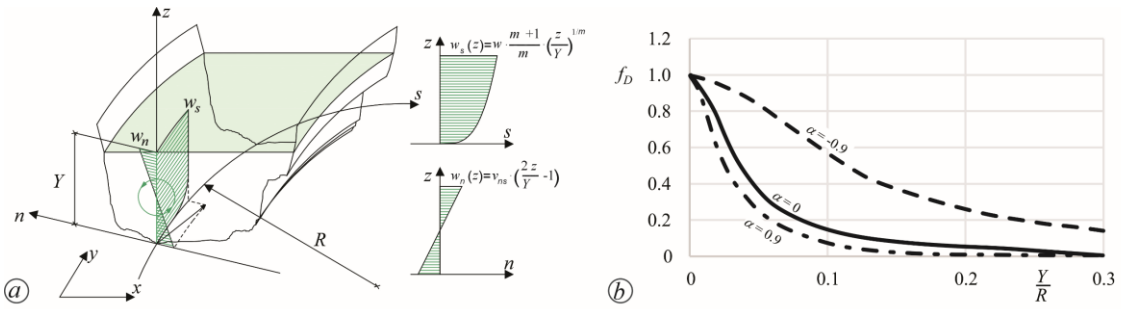

Figure 1. a) schematics of main and secondary flow in a channel bend, with notation; b) dampening factor, f_D, for $m = 7$ and for different value of the normalized transversal gradient of velocity, α.

2.2 *2D hydrodynamic model*

The previous equations were implemented in a 2D, depth-averaged, Finite Element model called "2DEF" (Defina, 2000, 2003; Viero et al. 2013; Mel et al., 2020a,b). It uses an unstructured, staggered, triangular mesh defined on a horizontal (x, y) Cartesian frame. The Manning-Strickler equation is used to model bed friction terms, which are treated semi-implicitly. The Reynolds stresses are modelled with the Boussinesq approximations, and the depth averaged formulation of Stansby (2003) is used for the eddy viscosity (Viero, 2019). The no-slip condition is prescribed at the side-walls using a wall function to estimate the lateral shear stress, which is added to the momentum balance of the boundary cells.

3 RESULTS AND DISCUSSION

The experiments of Blanckaert & de Vriend (2003) and Rozovskii (1957) are used to test the model effectiveness in reproducing the secondary flow in relatively sharp bends. The channels used for the experiments are schematically shown in Figure 2.

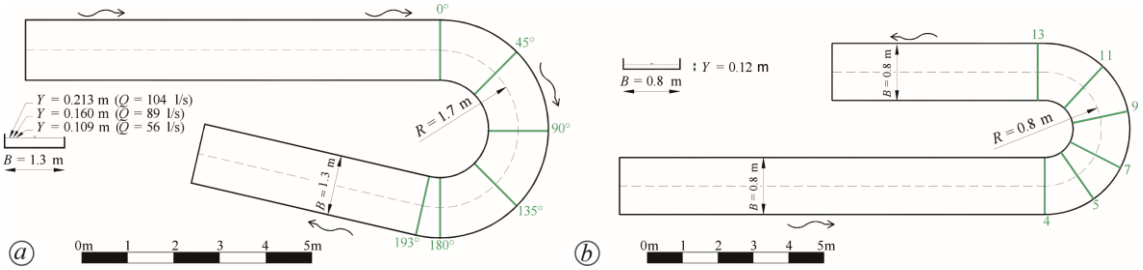

Figure 2. a) Laboratory flumes used by Blanckaert & de Vriend (2003) and b) by Rozovskii (1957).

3.1 *Blanckaert & de Vriend (2003) experiment*

Blanckaert & de Vriend (2003) performed experiments in the Ecole Polytechnique Fédérale Lausanne (EPFL), 19.7 m long and 1.3 m wide channel, with vertical sidewalls. The bottom is fixed and flat, and the Strickler coefficient is K_S = 60 m$^{1/3}$/s. The bend develops for 193° with a constant curvature (radius R = 1.7 m at the centreline). Three steady flow conditions were tested, with a discharge of 56, 89, and 104 l/s and a water depth of 10.9, 16.0, and 21.3 cm at the downstream section, respectively.

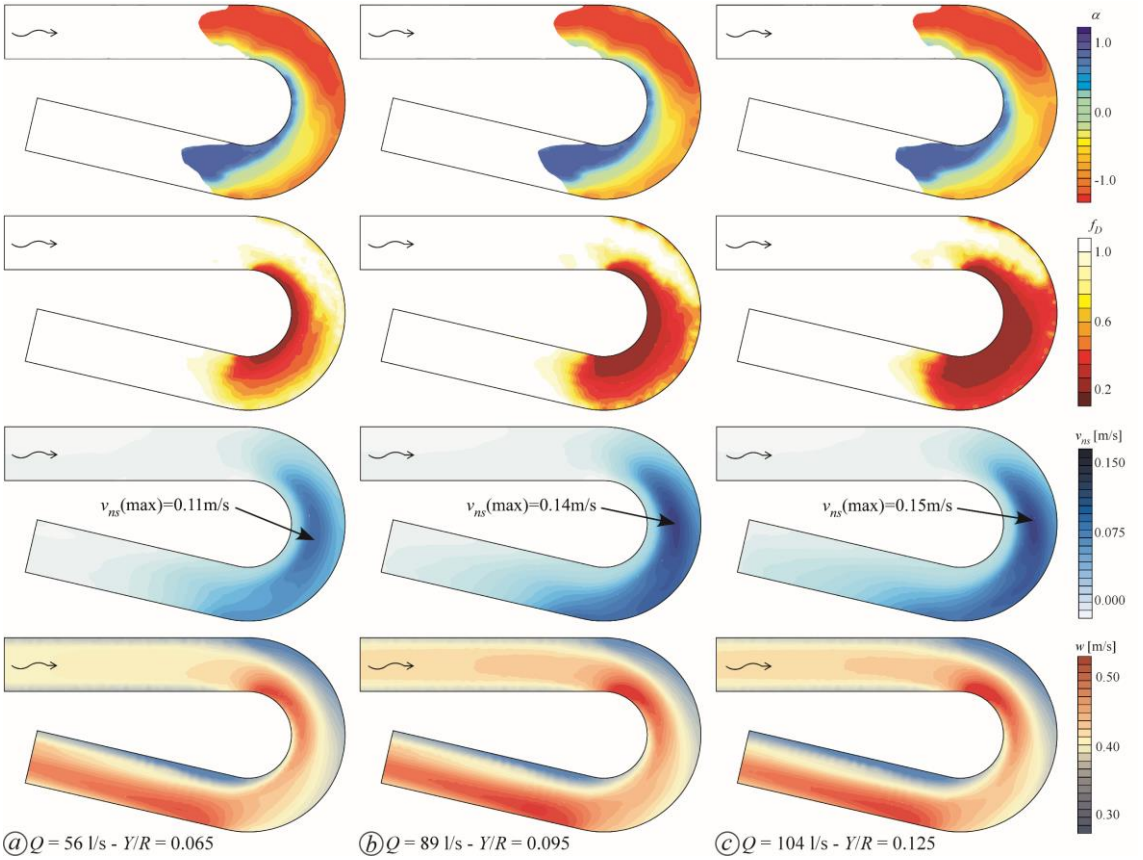

Figure 3. Spatial distribution of the normalized transversal gradient of velocity, α, of the dampening factor, f_D, and of the transversal velocity at the free surface, v_{ns}, for a) Q = 56 l/s, b) Q = 89 l/s, and c) Q = 104 l/s.

Figure 3, for the three different flowrates, shows the modelled spatial distribution of the normalized transversal gradient of velocity, α, of the dampening factor, f_D, of the helical flow

intensity in terms of transversal velocity at the free-surface, v_{ns}, and of the depth-averaged flow velocity, w. At the beginning of the bend, the high-velocity thread locates at the inner side (i.e., $\alpha < 0$) and there is no dampening of the vorticity production ($f_D \approx 1$). As the intensity of helical flow increases, momentum is redistributed by the secondary flow, the high-velocity thread is shifted towards the outer bank (α progressively reduces) and non-linear saturation effects starts hindering the growth of helical flow. At the downstream end of the bend, $\alpha \approx 1$, meaning that the secondary flow has moved the high-velocity close to the outer bank. By increasing the discharge and the water depth (hence the bend sharpness Y/R), v_{ns} increases faster, α reduces faster as well and, in turn, the non-linear saturation arises faster and stronger (f_D reduces faster, and to values closer to zero, for increasing discharges).

Figure 4 shows the secondary flow intensity at the channel centreline along the bend, expressed in terms of $\langle f_n^2 \rangle$, defined as (Blanckaert & de Vriend, 2003):

$$\langle f_n^{\,2} \rangle = \frac{\langle v_{ns}^2 \rangle}{\left(\frac{wY}{R}\right)^2} \tag{9}$$

where angle brackets denote depth-averaging. For the three available discharges, the measured data (dotted lines) are compared with the results from the linear model (i.e., with $f_D = 1$, dashed lines) and the non-linear model (with f_D spatially distributed as in Figure 3). While the linear model, which disregard the saturation effects, overestimates the secondary flow intensity significantly, the non-linear model nicely matches the experimental data.

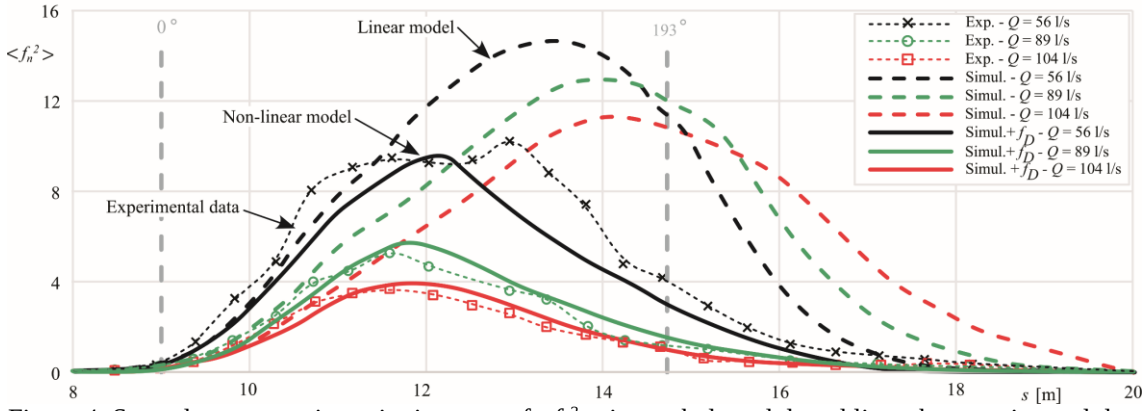

Figure 4. Secondary current intensity in terms of $\langle f_n^2 \rangle$; in symbols and dotted lines the experimental data (adapted from Blanckaert & de Vriend, 2003), in dashed lines the results of the linear model, in solid lines the results of the non-linear model (with f_D). Black lines and cross symbols are used for Q = 56 l/s, green lines and circle symbols are used for Q = 89 l/s, red lines and square symbols are used for Q = 104 l/s.

It is interesting to note that increasing the discharge and the water depth means increasing the bend sharpness (Y/R = 0.065, 0.095 and 0.125, respectively). The helical flow intensity increases accordingly (Figure 4), yet the depth-averaged flow fields show only minor changes (bottom row in Figure 3), as the outward momentum transfer, and the ensuing velocity redistribution, are counteracted by the saturation mechanism.

3.2 *Rozovskii (1957) experiment*

The experiment of Rozovskii (1957) has been performed in a U-shaped channel 11.5 m long, 80 cm wide and with vertical side walls. The bend develops for 180° with a constant curvature (radius R = 0.8 m at the centreline). The bottom is flat and fixed, with a Strickler coefficient K_S = 70 m$^{1/3}$/s. The inlet velocity is w = 0.26 m/s, and the water depth at the outlet is Y = 5.1 cm.

The measured data (red squares in Figures 5 and 6) are compared with the results from the model run without considering the dispersive stresses, from the linear, and from the non-linear model (solid lines). Without considering the dispersive terms in SWEs equations (dotted lines), the model overpredicts the velocity peak at the inner part of the bend (sections 5, 7, 9, and 11 in Figure 5), and the transverse tilting of the water surface slope is not well captured (Figure 6).

Including dispersive terms with a linear formulation (i.e., with $f_D = 1$, dash-dotted lines in Figures 5 and 6), together with the no-slip condition at the walls, shifts the high-velocity thread to the outer side of the bend exaggeratedly. The large streamwise slope of the free-surface along the bend is the result of excessive head losses ascribed to a marked confinement of the high velocity core close to the outer sidewall.

The non-linear model with the wall function for no-slip condition at the sidewalls (solid lines in Figures 5 and 6) well reproduces the measured data, in terms of both transversal distribution of streamwise velocity (Figure 5) and free-surface elevation along the inner and outer sidewalls (Figure 6).

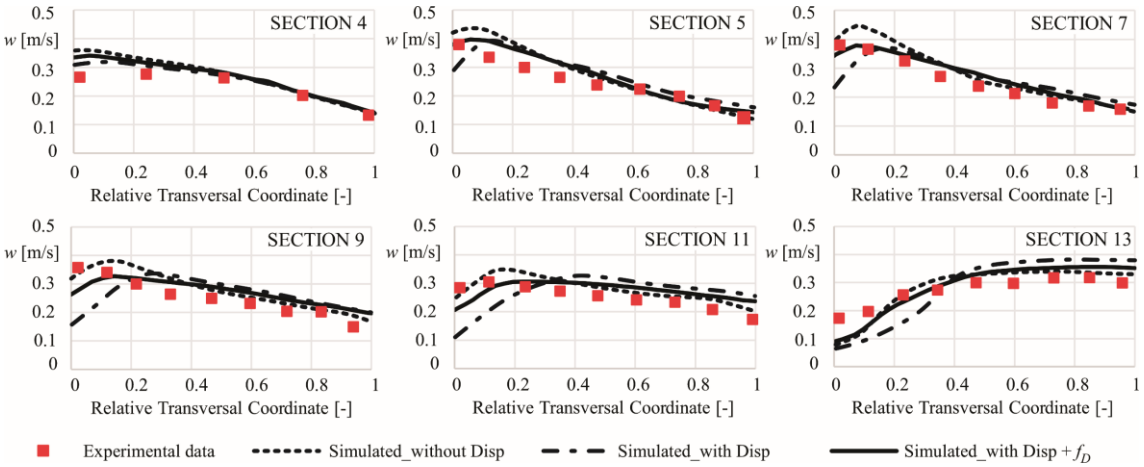

Figure 5. Transversal profiles of depth-averaged velocity for the Rozovskii (1957) experiment: measured data (red squares) are compared with the results of the model without dispersive terms (dotted lines), considering dispersive terms by means of a linear model (dash-dot lines) and of the non-linear model (dash-dot lines) with the spatially-distributed dampening factor, f_D. The relative transversal coordinate spans the channel width starting from the left bank.

The comparison between the linear and the non-linear models confirms a well-known issue (Johannesson & Parker, 1989; Blanckaert, 2001): the use of linear models for the secondary flow along with the no-slip condition at sidewalls in relatively sharp bends ($Y/R \approx 0.07$ in the Rozovskii experiment) leads to a marked overestimation of the helical flow intensity. The simplest choice commonly adopted to circumvent this problem is to relax the no-slip condition (Lien et al., 1999; Song et al., 2012). In this way, the shear stress actually acting at the sidewalls is disregarded, and an unphysical momentum flux is generated at the impervious banks that balances out the velocity redistribution. The present results suggest that accounting for non-linear saturation effect by means of a spatially distributed dampening factor overcomes this issue, limiting the excessive growth of the helical flow intensity in sharp bends and, at the same time, allowing the use of wall functions to account for sidewall shear stresses.

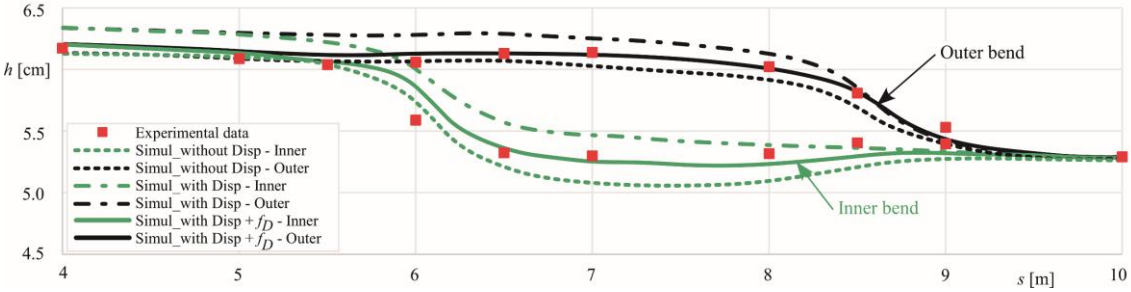

Figure 6. Longitudinal profile of water surface elevation at the inner bend (green lines) and at the outer bend (black lines): the red squares are the measured data (Rozovskii, 1957), the dotted lines represent the result of the model without dispersive terms, the dash-dot lines represent the result of the model considering dispersive terms; the filled lines represent the result of the model considering dispersive terms and the dampening factor f_D.

4 CONCLUSIONS

In this work, a model for secondary currents in curved channels is implemented in a general-purpose 2D shallow water model based on a Cartesian frame. The non-linear saturation effect, which emerges as a by-product of substantial velocity redistribution ascribed to secondary flow and limits the growth of helical flow intensity in sharper bends, is included by means of a pure 2D formulation. In the proposed model for secondary flow, there isn't any reference to channel width and centreline, nor to the distance from banks. The helical flow intensity is estimated by solving a transport equation for streamwise vorticity component, so as to account for inertia and phase-lag that characterize the growth and decay of the spiral motion. Yet, source and sink terms are all computed starting from local variables (flow depth and velocity, radius of curvature, and a friction coefficient).

Application to experimental case studies involving relatively sharp bends showed the effectiveness of the model and suggested that the no-slip condition at impervious bank can be accounted for without producing excessively strong secondary currents, as observed in previous applications of linear model for secondary currents.

Future activities should be devoted to test the model in real rivers, typically characterized by irregular boundaries, uneven bathymetries, and by the possible presence of floodplains.

REFERENCES

Begnudelli, L., Valiani, A., Sanders, B.F., 2010. A balanced treatment of secondary currents, turbulence and dispersion in a depth-integrated hydrodynamic and bed deformation model for channel bends. *Advances in Water Resources*, 33, 17–33. https://doi.org/10.1016/j.advwatres.2009.10.004

Blanckaert, K., 2001. Discussion of "Bend-Flow Simulation Using 2D Depth-Averaged Model". *Journal of Hydraulic Engineering*, 127, 167–170. https://doi.org/10.1061/(ASCE)0733-9429(2001)127:2(167)

Blanckaert, K., 2009. Saturation of curvature-induced secondary flow, energy losses, and turbulence in sharp open-channel bends: Laboratory experiments, analysis, and modeling. *Journal of Geophysical Research: Earth Surface*, 114. https://doi.org/10.1029/2008JF001137

Blanckaert, K., de Vriend, H.J., 2010. Meander dynamics: A nonlinear model without curvature restrictions for flow in open-channel bends. *Journal of Geophysical Research: Earth Surface*, 115. https://doi.org/10.1029/2009JF001301

Blanckaert, K., de Vriend, H.J., 2003. Nonlinear modeling of mean flow redistribution in curved open channels. *Water Resources Research*, 39. https://doi.org/10.1029/2003WR002068

Camporeale, C., Perona, P., Porporato, A., Ridolfi, L., 2007. Hierarchy of models for meandering rivers and related morphodynamic processes. *Reviews of Geophysics*, 45. https://doi.org/10.1029/2005RG000185

Defina, A., 2000. Two-dimensional shallow flow equations for partially dry areas. *Water Resources Research*, 36, 3251–3264. https://doi.org/10.1029/2000WR900167

Defina, A., 2003. Numerical experiments on bar growth. *Water Resources Research*, 39, 1092. https://doi.org/10.1029/2002WR001455

Johannesson, H., Parker, G., 1989. Secondary Flow in Mildly Sinuous Channel. *Journal of Hydraulic Engineering*, 115, 289–308. https://doi.org/10.1061/(ASCE)0733-9429(1989)115:3(289)

Lien, H.C., Hsieh, T.Y., Yang, J.C., Yeh, K.C., 1999. Bend-Flow Simulation Using 2D Depth-Averaged Model. *Journal of Hydraulic Engineering*, 125, 1097–1108. https://doi.org/10.1061/(ASCE)0733-9429(1999)125:10(1097)

Mel, R., Viero, D.P., Carniello, L., D'Alpaos, L., 2020a. Multipurpose Use of Artificial Channel Networks for Flood Risk Reduction: The Case of the Waterway Padova–Venice (Italy). *Water*, 12, 1609. https://doi.org/10.3390/w12061609

Mel, R.A., Viero, D.P., Carniello, L., D'Alpaos, L., 2020b. Optimal floodgate operation for river flood management: The case study of Padova (Italy). *Journal of Hydrology-Regional Studies*, 30, 100702. https://doi.org/10.1016/j.ejrh.2020.100702

Odgaard, A.J., 1986. Meander Flow Model. I: Development. *Journal of Hydraulic Engineering*, 112, 1117–1135. https://doi.org/10.1061/(ASCE)0733-9429(1986)112:12(1117)

Ottevanger, W., 2013. Modelling and parametrizing the hydro- and morphodynamics of curved open channels. *PhD Thesis*, Delft University of Technology, The Netherlands. https://doi.org/10.4233/uuid:9f19d0ea-5d89-4c15-b99d-3fb02fc28eb7

Qin, C., Shao, X., Xiao, Y., 2019. Secondary Flow Effects on Deposition of Cohesive Sediment in a Meandering Reach of Yangtze River. *Water*,11. https://doi.org/10.3390/w11071444

Rozovskii, I.L., 1957. Flow of water in bends of open channels. *Academy of Sciences of the Ukrainian SSR*. English translation: Israel Progr. for Scientific Transl., Monson, Jerusalem, Israel, 1961

Song, C.G., Seo, I.W., Kim, Y.D., 2012. Analysis of secondary current effect in the modeling of shallow flow in open channels. *Advances in Water Resources*, 41, 29–48. https://doi.org/10.1016/j.advwatres.2012.02.003

Stansby, P.K., 2003. A mixing length model for shallow turbulent wakes. *Journal of Fluid Mechanics*, 495, 369–384. https://doi.org/10.1017/S0022112003006384

Viero, D.P., 2019. Modelling urban floods using a finite element staggered scheme with an anisotropic dual porosity model. *Journal of Hydrology*, 568, 247–259. https://doi.org/10.1016/j.jhydrol.2018.10.055

Yeh, K., Kennedy, J.F., 1993. Moment Model of Nonuniform Channel-Bend Flow. I: Fixed Beds. *Journal of Hydraulic Engineering*, 119, 776–795. https://doi.org/10.1061/(ASCE)0733-9429(1993)119:7(776)